Hindawi
Advances in Civil Engineering
Volume 2018, Article ID 3497390, 18 pages
https://doi.org/10.1155/2018/3497390

Research Article

Parametric Study on Mixed Torsional Behavior of U-Shaped Thin-Walled RC Girders

Jianchao Xu,[1] **Bo Diao**,[2,3] **Quanqan Guo**,[4] **Yinghua Ye**,[2,3] **Y. L. Mo**,[5] **and Tianmin Zhou**[6]

[1]*Ph.D. Candidate, School of Transportation Science and Engineering, Beihang University, Beijing 100191, China*
[2]*Dr. Professor, School of Transportation Science and Engineering, Beihang University, Beijing 100191, China*
[3]*State Laboratory of Subtropical Building Science, South China University of Technology, Guangzhou 510640, China*
[4]*Dr. Associate Professor, School of Transportation Science and Engineering, Beihang University, Beijing 100191, China*
[5]*Dr. Professor, Department of Civil and Environmental Engineering, University of Houston, Houston, TX 77204-4003, USA*
[6]*Ph.D. Student, Department of Civil and Environmental Engineering, University of Houston, Houston, TX 77204-4003, USA*

Correspondence should be addressed to Quanquan Guo; qq_guo@buaa.edu.cn

Received 12 June 2018; Accepted 19 September 2018; Published 15 November 2018

Academic Editor: Eric Lui

Nowadays, U-shaped thin-walled concrete girders have been widely applied in the urban construction of rail viaducts in China as well as worldwide. However, the mixed torsional behaviors of these structures are not well understood. In this paper, the mixed torsional behaviors of the U-shaped thin-walled RC girders are theoretically analyzed, and a method predicting failure modes and ultimate torques is proposed. Nonlinear FE models based on ABAQUS to simulate the mixed torsional behaviors are built and calibrated with the test results. Parametric studies considering three crucial parameters (boundary condition, span length-section height ratio, and ratio of longitudinal bars to stirrups) are conducted based on both the above suggested calculating method and the FE modeling. The calculated and the simulated results agree well with each other and with the test results. It is found that the failure modes of the U-shaped thin-walled RC girders under torsion are influenced by all the three parameters. Three kinds of failure modes are observed: flexural failures dominated by warping moment, shear failures caused by warping torque and circulatory torque, and flexural-shear failures in the cases where flexural failure and shear failure appear almost at the same time.

1. Introduction

U-shaped thin-walled concrete girders are composed of two webs and a bottom slab, with trains travelling through inside [1–4]. Comparing with traditional girders like box girders, U-shaped thin-walled girders have some advantages such as lower construction elevation (since trains travel inside), easier power system layout (since there is enough space inside for the power system), and attractive appearance. For the U-shaped thin-walled RC girders, torsion is a critical factor considering the transverse wind load and the eccentric traffic load (in multilane cases and curved structure cases).

The elastic torsional response of an open thin-walled structure was first formulated by Vlasov in 1961 [5]. Then, some improvements on Vlasov's theory have been made for some specific cases such as focusing on the shear deformation caused by warping torque [6, 7] or focusing on the secondary warping effect [8]. According to Vlasov's theory, when an open thin-walled structure is under torsion, it is a mixed torsional case of circulatory torsion and warping torsion. Three kinds of internal forces exist simultaneously, which are circulatory torque T_c (comes from circulatory torsion), warping torque T_ω, and warping moment M_ω (come from warping torsion).

The postcracking circulatory torsional behavior of RC closed-section structures has been well simulated with the space truss model [9–16]. The nonlinear FEA method was also applied to simulate the circulatory torsional behavior of

RC closed-section structures [17–19]. As to the postcracking mixed torsional behavior of open thin-walled RC structures, the aforementioned space truss model for circulatory torsion is not accurate anymore due to the considerable warping effect [3, 20]. In 1968, the postcracking mixed torsional behavior of a U-shaped thin-walled RC girder was first addressed [21]. Then in 1981, the mixed torsional behavior of a large U-shaped thin-walled RC girder was systematically tested (with both ends fixed) and analyzed by Krpan and Collins [22, 23]. Although immature anchoring failure occurred, the test results clearly showed the dominating role that warping moment played. In 1983, Hwang and Hsu proposed a nonlinear analysis model based on the Fourier series approach to simulate the mixed torsional behavior of U-shaped thin-walled RC girders [1]. Apart from the U-shaped thin-walled RC girders, the I-shaped RC girders are also open section members applied in Civil Engineering, although their warping effect is not very strong. In 1991, the combined torsional and flexural behaviors of eight I-shaped RC girders were experimentally and analytically studied [20], and a method to calculate the ultimate load was suggested by modifying the skew bending theory [24]. In the following three decades, few research outcomes on the mixed torsional behaviors of U-shaped thin-walled RC girders were reported in the literature. In the 21st century, their torsional performance has again been addressed due to their wide application in rail viaduct engineering. In 2016, three large fixed-fixed U-shaped thin-walled RC girders were tested and analyzed by Chen et al. [3, 25]. Flexural failures dominated by the warping moment were observed for all the girder specimens, based on which a simple method to calculate the ultimate torques was proposed, where only the warping moment was taken into account.

As listed above, the current research outcomes on the mixed torsional behavior of U-shaped thin-walled RC girders are derived from a limited number of experimental or analytical studies. The torsional behavior of such girders is still unclear. A comprehensive parametric study is needed to thoroughly understand the mixed torsional behavior of such structures. In this paper, the mixed torsional behavior of these girders is first theoretically analyzed based on Vlasov's theory, and a method able to calculate both the failure mode and the ultimate torque is derived. Since in modern research the structural engineering finite element analysis (FEA) is essential for supplementing experimental investigations [26, 27], nonlinear FE modeling based on ABAQUS is carried out. Finally, a comprehensive parametric study based on both proposed calculating method and FE modeling is performed considering three crucial parameters, i.e., boundary condition, span-height ratio, and ratio of longitudinal bars to stirrups.

2. Theoretical and Ultimate Equilibrium Analyses

2.1. Theoretical Analysis. The theoretical analysis is performed based on Vlasov's theory [5], and two typical distributions of internal forces are shown in Figure 1(a) (fixed-fixed supported case) and Figure 1(b) (simply supported case), respectively. The simply supported boundary condition here means that the rotation of the girder end is constrained but the girder end is free to warp in the longitudinal direction. According to Vlasov's theory [5], the corresponding formula of the internal forces in the two boundary conditions are given in Equations (1) (fixed-fixed supported) and (2) (simply supported), respectively, where M_ω is the warping moment; T_ω is the warping torque; T_c is the circulatory torque; k is the characteristic length defined as the square root of the stiffness ratio of warping torsion to circulatory torsion, $k = \sqrt{(EI_\omega)/(GK)}$ (m); E is the elasticity modulus; I_ω is the principal sectorial moment of inertia calculated by $I_\omega = \int_A \omega^2\, dA$, in which ω is principal sectorial coordinate; G is the shear modulus taken as $0.4E$; K is St. Venant's torsional constant; L is the span length; and "sinh" and "cosh" are the hyperbolic sine and the hyperbolic cosine functions, respectively. It should be noted that, in the mixed torsional cases, the characteristic length k is a key cross-sectional property, and for the U-shaped thin-walled RC girder studied in this paper, it has a value of 2.06 m, which is 4.12 times the section height. The characteristic length k is discussed in detail in Section 5.4:

$$\begin{cases} M_\omega(z) = 0.5Tk\dfrac{\cosh(z/k) - \cosh((0.5L - z)/k)}{\sinh(0.5L/k)}, & (0 \le z \le 0.5L), \\ T_\omega(z) = 0.5T\dfrac{\sinh(z/k) + \sinh((0.5L - z)/k)}{\sinh(0.5L/k)}, & (0 \le z \le 0.5L), \\ T_c(z) = 0.5T - T_\omega(z), & (0 \le z \le 0.5L), \end{cases} \tag{1}$$

$$\begin{cases} M_\omega(z) = 0.5Tk\dfrac{\sinh(z/k)}{\cosh(0.5L/k)}, & (0 \le z \le 0.5L), \\ T_\omega(z) = 0.5T\dfrac{\cosh(z/k)}{\cosh(0.5L/k)}, & (0 \le z \le 0.5L), \\ T_c(z) = 0.5T - T_\omega(z), & (0 \le z \le 0.5L). \end{cases} \tag{2}$$

It can be seen from Figures 1(a) and 1(b) and Equations (1) and (2) that the total internal torque $0.5T$ is the sum of warping torque T_ω and circulatory torque T_c. Moreover, like the relationship between bending moment and shear force, the warping torque T_ω is the differential formula of the warping moment M_ω. For the fixed-fixed supported case, warping moment M_ω and warping torque T_ω reach the maximum at support and midspan, while circulatory torque T_c reaches its maximum at quarter span. As to the simply supported case, warping moment M_ω and warping torque T_ω reach their maximum at midspan, whereas the maximum circulatory torque T_c exists at support. The distributions of warping normal stress, warping torsional shear stress, and circulatory torsional shear stress are shown in Figure 1(c). As shown in Figure 1(c), warping normal stress antisymmetrically distributes around the U-shaped section. Warping torsional shear flow flows along the centerline of the U-shaped section, while the circulatory torsional shear flow forms a U-shaped circle. According to the distributions of internal forces discussed above, at ultimate state, two kinds of potential failure may occur, namely, a flexural failure

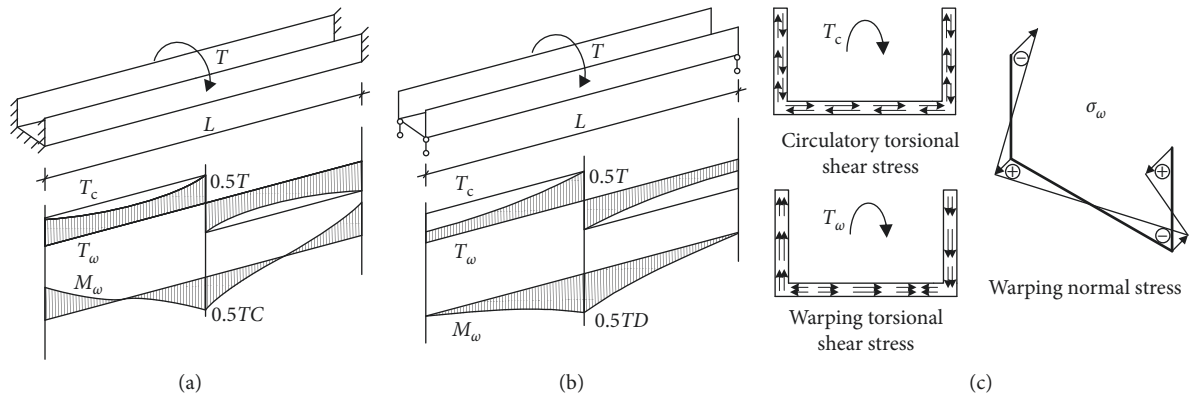

Figure 1: Distributions of internal forces and the corresponding stresses: (a) internal forces in a fixed-fixed supported case, (b) internal forces in a simply supported case, and (c) stress distributions. Note: $C = 0.5Tk([\cosh(0.5L/k) - 1]/\sinh(0.5L/k))$; $D = 0.5Tk \cdot \sinh(0.5L/k)/\cosh(0.5L/k)$.

dominated by warping moment (in the fixed-fixed supported case, it occurs at midspan and support, while in the simply supported case, it occurs at midspan) and a shear failure dominated by the combined action of circulatory torque and warping torque (in the fixed-fixed supported case, it occurs at quarter span, while in the simply supported case, it occurs at support). The potential shear failure occurs at the location where the maximum circulatory torque T_c appears because the U-shaped thin-walled section is weaker at resisting circulatory torque T_c than resisting warping torque T_ω due to the small circulatory torsional lever arm.

When the ultimate state is the concern, more attention should be paid to the maximum values of internal forces. Referring to Equations (1) and (2), noting $\gamma = L/k$ (ratio of span length to characteristic length), the maximum internal forces in the fixed-fixed supported case and in the simply supported case can be, respectively, expressed in Equations (3) and (4), where "tanh" is hyperbolic tangent function:

$$\begin{cases} M_{\omega,\max} = 0.5Tk\left(\dfrac{[\cosh(0.5\gamma) - 1]}{\sinh(0.5\gamma)}\right), \\ T_{\omega,\max} = 0.5T, \\ T_{c,\max} = 0.5T\left[1 - \dfrac{2\sinh(0.25\gamma)}{\sinh(0.5\gamma)}\right], \end{cases} \tag{3}$$

$$\begin{cases} M_{\omega,\max} = 0.5Tk\tanh(0.5\gamma), \\ T_{\omega,\max} = 0.5T, \\ T_{c,\max} = 0.5T\left[1 - \dfrac{1}{\cosh(0.5\gamma)}\right]. \end{cases} \tag{4}$$

The relationship between the maximum internal forces and γ in Equations (3) and (4) are visualized in Figure 2. It can be seen that, for both fixed-fixed supported and simply supported cases, with the increase of γ, warping moment M_ω and circulatory torque T_c have the upper limit values of 0.5 Tk and 0.5 T, respectively. Moreover, they increase much

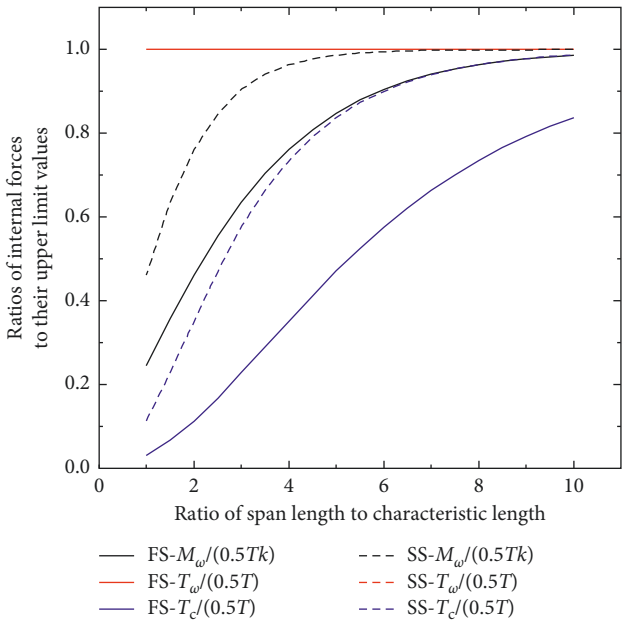

Figure 2: Variation tendency of the maximum internal forces with the increasing of span length. "FS" and "SS" mean "fixed-fixed supported" and "simply supported," respectively.

faster in the simply supported case than in the fixed-fixed supported case. Besides, it can be observed from Figure 2 that, in both fixed-fixed and simply supported cases, when the span length-characteristic length ratio γ is small, warping torque T_ω dominates, while warping moment M_ω and circulatory torque T_c have small values; thus shear failure dominated by warping torque may occur. When γ has a medium value, warping moment M_ω dominates and flexural failure dominated by warping moment may occur. When γ has a large value, circulatory torque T_c dominates, and shear failure dominated by circulatory torque may occur.

2.2. Ultimate Equilibrium Analysis. Ultimate equilibrium analyses for the two abovementioned potential failures are

conducted here. As stated in the literature review, the flexural failures dominated by warping moment were experimentally observed and theoretically calculated by Chen et al. [3]. In this paper, a calculating method for the potential shear failure is proposed. Moreover, the calculating method for the flexural failure suggested by Chen et al. will be improved by taking the shear effect of warping torque into consideration.

2.2.1. Calculation of the Potential Flexural Failure. As shown in Figures 1(a) and 1(b), apart from the maximum warping moment M_ω, the warping torque T_ω also exists at the flexural critical segments. Thus, the calculation method of flexural failure only considering warping moment [3] is modified here by taking the warping torque into account. As shown in Figure 1(c), the warping moment M_ω is a self-balanced internal force; thus at ultimate state, the warping effect is considered on three separated rectangular thin walls. As shown in Figure 3, every thin wall is equivalently subjected to a bending moment, and the equivalent bending moment on the right web can be obtained by $M_{\text{eq}} = \int_A \sigma_\omega y_1 \, dA$. As to the treatment of warping torque T_ω, as shown in Figure 1(c), the warping torque is totally resisted by the warping torsional shear stresses on the two webs, while the warping torsional shear stress in the bottom slab makes no contribution due to its self-counteraction. Therefore, at the ultimate state, the warping torque is considered equivalent to a couple of shear forces $V_\omega = T_\omega / d_{\text{w}}$ on the two webs acting in opposite directions, where d_{w} is the distance between the centerlines of two webs. Considering Equation (3) and $\sigma_\omega = M_\omega \omega / I_\omega$, defining $\eta_1 = \int_A \omega y_1 \, dA$, then for the fixed-fixed supported case, the equivalent shear force and bending moment on the webs can be expressed by

$$\begin{cases} V_\omega = \dfrac{0.5T}{d_\omega}, \\ \\ M_{\text{eq}} = 0.5Tk\eta_1 \left[\dfrac{[\cosh(0.5\gamma) - 1]}{[I_\omega \sinh(0.5\gamma)]} \right]. \end{cases} \tag{5}$$

Considering Equation (4) for the simply supported case, they can be expressed by

$$\begin{cases} V_\omega = \dfrac{0.5T}{d_\omega}, \\ \\ M_{\text{eq}} = \dfrac{0.5Tk \tanh(0.5\gamma)\eta_1}{I_\omega}. \end{cases} \tag{6}$$

At the ultimate state as shown in Figure 4(a), the shear force is resisted by the tension in reinforcement and the compression in the diagonal concrete struts [15, 24], and the tangential equilibrium can be expressed by Equation (7). The normal equilibrium on the web is shown in Figure 4(b), and it can be expressed by Equation (8) referring to the calculation method of bending-shear capacities of shear walls [28]:

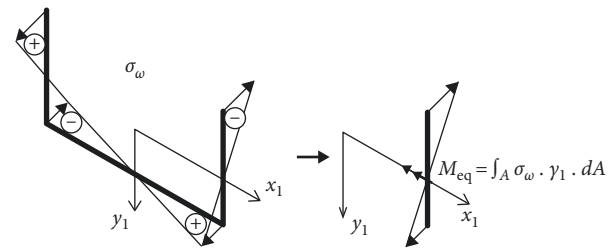

Figure 3: Distributing method for warping moment.

$$V_\omega = \frac{2F_{\text{ty1}} h_0 \cot(\theta)}{s}, \tag{7}$$

$$\begin{cases} 0 = \dfrac{f_{\text{lu}} A_{\text{s}} + f_{\text{lu}} A_{\text{sd}} (h_0 - 1.5x)}{h_{\text{d}}} - 0.85 f_{\text{c}} bx - f'_{\text{ly}} A'_{\text{s}} - V_\omega \cot(\theta), \\ \\ M_{\text{eq}} = f_{\text{lu}} A_{\text{s}} (h_0 - 0.5x) + f_{\text{lu}} \left[\dfrac{A_{\text{sd}} (h_0 - 1.5x)}{h_{\text{d}}} \right] (0.5h_0 + 0.25x) \\ \qquad + f'_{\text{ly}} A'_{\text{s}} (0.5x - a') - V_\omega \cot(\theta) (0.5h_0 - 0.5x), \end{cases} \tag{8}$$

where F_{ty1} is the yielding force of one stirrup leg; s is the stirrup spacing; f_{lu} and f'_{ly} are the ultimate tensile stress and yielding compressive stress (absolute value) of the longitudinal bars, respectively; A_{sd} is the area of all distributing bars; and x is the depth of a concrete equivalent rectangular stress block with a uniform compressive stress of $0.85 f_{\text{c}}$ [29]. Since the stress near the neutral axis is low, only the distributing bars located beyond $1.5x$ (expressed as $A_{\text{sd}} (h_0 - 1.5x)/h_d$) are considered to contribute to the tensile resistance. Then, the ultimate torque of the potential flexural failure can be solved by combining Equations (7), (8), and (5) or (7), (8), and (6) for the fixed-fixed supported case or for the simply supported case, respectively.

2.2.2. Calculation of the Potential Shear Failure. A method to calculate the shear failure in this mixed torsional case is developed here based on the skew bending theory, also called the plastic truss model [15, 24]. At the ultimate state as shown in Figure 5(a), the circulatory torsional shear flow q_{c} can be obtained as $q_{\text{c}} = T_{\text{c}} / (2A_0)$, where A_0 is the area enclosed by the shear flow, and it is assumed that the center line of the shear flow coincides with the inner face of the stirrup. The warping torsional shear flow q_ω on the webs can be expressed by $q_\omega = T_\omega / (2d_{\text{w}} d_1)$. Under the combined action of warping torque and circulatory torque, the two webs are more critical than the bottom slab due to the interaction of the two kinds of shear flows. The ultimate equilibrium on the right web of the U-shaped girder is shown in Figure 5(b), where the shear flows due to circulatory and warping torques are additive on the right side, while are subtractive on the left side. On the top and bottom sides, only circulatory torsional shear flow exists. The combined shear flows can be obtained as

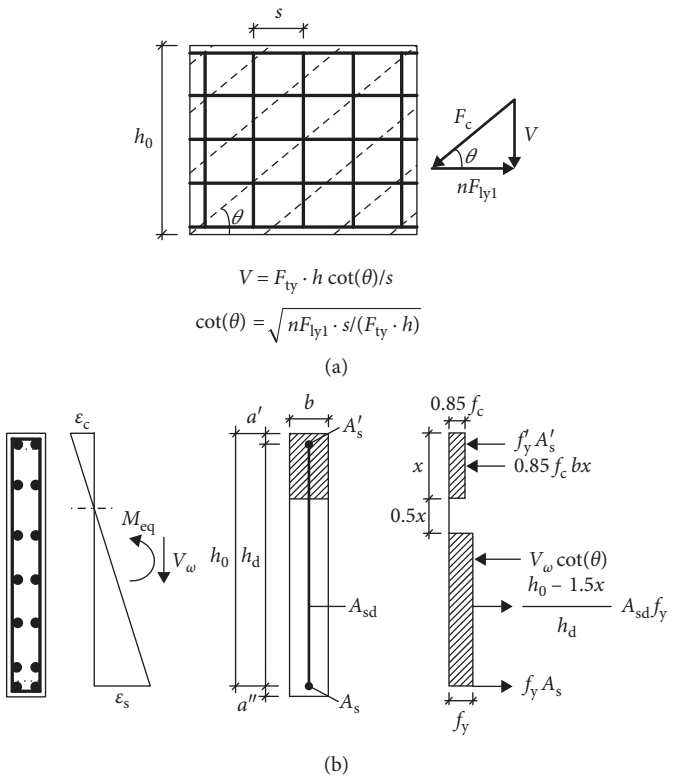

Figure 4: Ultimate equilibriums under the combined actions of warping moment and warping torque: (a) the truss model bearing the equivalent shear force and (b) ultimate equilibrium in the normal direction.

$$\begin{cases} q_1 = q_c + q_\omega, \\ q_3 = q_c - q_\omega, \\ q_2 = q_4 = q_c. \end{cases} \tag{9}$$

Considering Equation (3), for the fixed-fixed supported case,

$$\begin{cases} q_1 = \left(0.5T \dfrac{[1 - 2\sinh(0.25\gamma)/\sinh(0.5\gamma)]}{(2A_0)}\right) \\ \qquad + \left(0.5T \dfrac{[2\sinh(0.25\gamma)/\sinh(0.5\gamma)]}{(2d_w d_1)}\right), \\ q_2 = q_4 = 0.5T \dfrac{[1 - 2\sinh(0.25\gamma)/\sinh(0.5\gamma)]}{(2A_0)}. \end{cases} \tag{10}$$

Considering Equation (4), for the simply supported case,

$$\begin{cases} q_1 = \left(0.5T \dfrac{[1 - 1/\cosh(0.5\gamma)]}{(2A_0)}\right) + \left(\dfrac{0.5T/\cosh(0.5\gamma)}{(2d_w d_1)}\right), \\ q_2 = q_4 = 0.5T\left(\dfrac{[1 - 1/\cosh(0.5\gamma)]}{(2A_0)}\right). \end{cases} \tag{11}$$

The web fails with the yielding of reinforcement on the right, top, and bottom sides, and at the ultimate state, the equilibrium is expressed as

$$\begin{cases} q_i = \dfrac{F_{ty1}\cot(\theta_i)}{s}, \quad i = 1, 2, 4, \\ 0 = f_{ly} A_{sr} d_2 - q_1 d_1 d_2 \cot(\theta_1) - 0.5 q_2 d_2^2 \cot(\theta_2) \\ \qquad - 0.5 q_4 d_2^2 \cot(\theta_4), \end{cases} \tag{12}$$

where A_{sr} is the area of the longitudinal bars on the right side of the web and f_{ly} is the yielding strength of the longitudinal bars. The ultimate torque of the potential shear failure can then be calculated by combining Equations (12) and (10) or (12) and (11) for the fixed-fixed supported case or for the simply supported case, respectively. The angle θ should not be less than 30° [29], in case that the longitudinal bars cannot reach yielding because of overreinforcement. If the solved angle $\theta < 30°$, the ultimate torque can be simply obtained by setting $\theta = 30°$.

3. Mixed Torsional Tests

The mixed torsional tests of U-shaped thin-walled RC girders are introduced here [3]. The detailed dimensions and reinforcing arrangements are shown in Figures 6(a) and 6(b), respectively. The total length, span length, section height, section width, and wall thickness of the tested girders were 7350 mm, 6650 mm, 500 mm, 900 mm, and 70 mm, respectively. The girder specimens were lengthened with solid strengthened blocks at the two ends to restrain warping

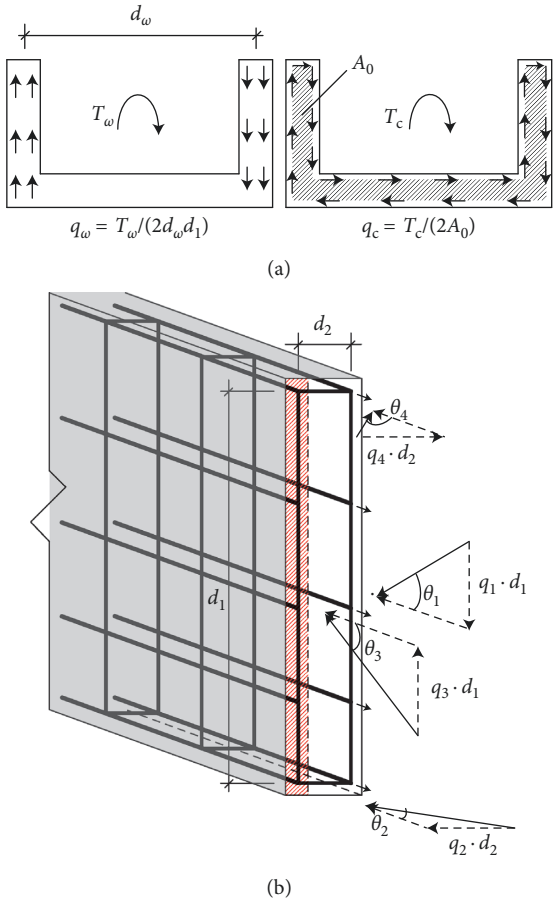

Figure 5: Ultimate equilibrium under the combined actions of warping torque and circulatory torque: (a) simplified distribution of torsional shear stresses and (b) ultimate equilibrium on the right web of the U-shaped girder.

deformation. A strengthened diaphragm was set at midspan to prevent local failure caused by loading. The material mechanical properties of the girder specimens (numbered as MEM-1, MEM-2, and MEM-3) are summarized in Table 1. In the loading test, the girder specimens were fixed at two ends and the concentrated torque T was introduced at midspan by two jacks acting upward and downward, referring to Figure 7.

During the test, similar experimental phenomenon was observed for all the specimens. The crack pattern on the external surface of the downward web (the web going down in the loading process) is shown in Figure 8. Referring to Figure 8, vertical flexural-type cracks dominated by warping moment occurred first at the support and midspan segments. Then inclined cracks appeared and developed over almost the whole span, with flexural-shear cracks at 1/8 and 3/8 segments, while web shear cracks at the quarter segment. Moreover, diagonal cracks on the external surfaces of the webs appeared earlier and developed more intensively than those on the internal surfaces of the webs, and it is due to that the two kinds of shear flows (Figure 1(c)) flow in the same direction on the external surfaces while in the opposite direction on the internal surfaces. Longitudinal bars yielded first at midspan and support while stirrups yielded afterwards at the quarter span. Finally, concrete crushing was observed at the support and midspan and flexural-type failure occurred.

The ultimate torques of the above girder specimens are calculated with the method proposed in Section 2.2. The calculated results together with the test results are compared in Table 2. The tested and calculated ultimate torques of the U-shaped thin-walled RC girder tested by Krpan and Collins [22] are also compared in Table 2 (numbered as MEM-Krpan). The smaller one between the calculated ultimate torques based on the potential flexural failure and potential shear failure is the true ultimate torque. It can be seen from Table 2 that the above proposed calculating method can give good predictions of the ultimate torques (with an average test/calculation value of 1.08) and the failure modes.

4. Nonlinear Finite Element Simulation

The commercial FEA program ABAQUS is applied to build the 3D FEA model to simulate the mixed torsional behavior of the U-shaped thin-walled RC girders, which is shown in Figure 7. Elements C3D8R are used for concrete to avoid the shear locking effect [30]. Elements T3D2 are used to model reinforcements. Two concrete elements are used through the thickness of the 70 mm thin walls considering that the circulatory torsional shear flow flows around the thin wall. Perfect bond is assumed between the concrete and reinforcement, using the embedded method. The torsional loading setup in this FE model is designed as the testing setup [3]. The bottom surfaces of the steel support frames are restrained by $U_1 = U_2 = U_3 = 0$. Surface to surface contacts are introduced between the support frames and the girder ends with the normal behavior of "hard" contact and tangential behavior of penalty friction formulation (the friction coefficient is set as 0.3). It is the same contact definition between the steel loading frame and the girder midspan. The external torque is introduced at the midspan by a couple of concentrated forces acting downward and upward. In this FE model, displacement control is applied with two equal displacements going downward at Reference Point 1 (RP1) and going upward at Reference Point 2 (RP2).

4.1. Material Modeling. The behavior of concrete can be modeled in ABAQUS with the concrete damage plasticity (CDP) model [18, 26, 27, 30, 31]. The CDP model was first proposed by Lubliner et al. [32] and then modified by Lee and Fenves [33, 34]. To define the CDP model, the uniaxial constitutive laws of concrete under compression and tension together with five constitutive parameters are required. Since only compressive strength and Young's modulus of concrete were reported in the test [3], as shown in Figure 9(a), the unconfined concrete uniaxial compressive stress-strain curve suggested by Mander et al. [35] is adopted, where $\varepsilon_0 = 2f_c/E_0$. In tension, the behavior of concrete is assumed to be linearly elastic up to the onset of cracking and then followed by tension softening. In this paper as shown in Figure 9(b), the stress-displacement curve suggested by the

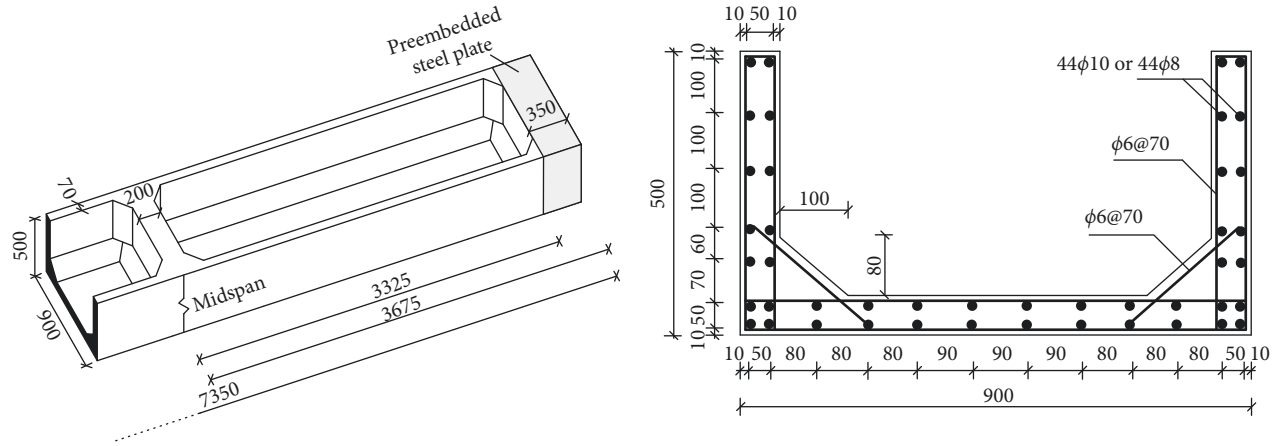

(a) (b)

Figure 6: Detailed information of the U-shaped thin-walled RC girder specimens (unit: mm): (a) dimensions and (b) reinforcing arrangements.

Table 1: Material properties of the girder specimens.

		MEM-1	MEM-2	MEM-3
Longitudinal bars	Yield strength (MPa)	576.2	353.3	353.3
	Ultimate strength (MPa)	623.0	573.3	573.3
	Diameter (mm)	10	8	8
Stirrups	Yield strength (MPa)	365.0	276.7	276.7
	Ultimate strength (MPa)	645.0	446.7	446.7
	Diameter (mm)	6	6	6
	Spacing (mm)	70	70	70
Concrete	Compressive strength (MPa)	51.0	63.8	51.6
	Elastic modules (GPa)	38.5	42.2	34.4

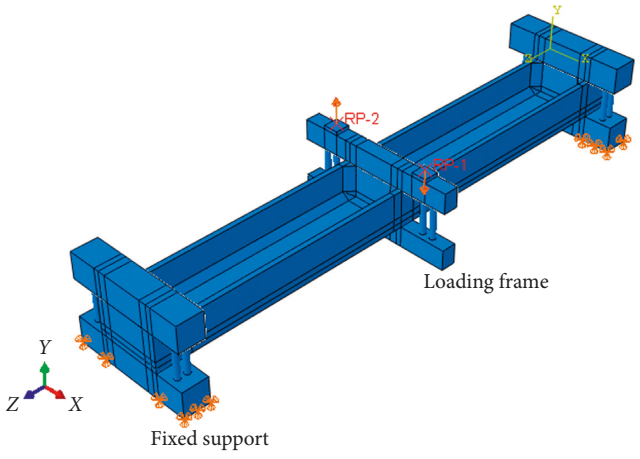

Figure 7: FE modeling of the U-shaped thin-walled RC girder under pure torsion.

CEB code [36] is applied. The fracture energy is calculated by $G_f = 73(f_{cm})^{0.18}$, where f_{cm} is the mean compressive strength. The tensile strength of concrete is determined by $f_{tm} = 0.3(f_{ck})^{2/3}$ [36], where f_{ck} is the characteristic value

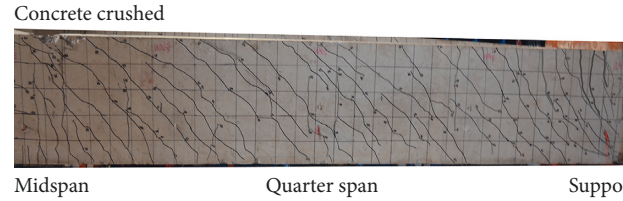

Figure 8: Test photo of the crack pattern on the external surface of the downward web.

Table 2: Comparison of the calculated and tested ultimate torques.

Girders	Ultimate torque (kNm)			Test/calculation
	Test	Calculation		
		Flexural failure	Shear failure	
MEM-1	199.7	**200.7**	208.2	0.99
MEM-2	151.0	**133.1**	135.8	1.13
MEM-3	147.0	**131.5**	135.8	1.12
MEM-Krpan	266.0	**249.5**	260.3	1.07
Average value				1.08
Standard deviation				0.07
Coefficient of variation				6.5%

of compressive strength ($f_{ck} = f_{cm} - 8$ (in MPa)). The five constitutive parameters are given in Table 3. Since no relative information is available from the experimental tests, default values of the five constitutive parameters [30] are used except for the viscosity parameter. As suggested by Lee and Fenves [34], the value of the viscosity parameter can be set at about 15% of one time increment in order for the solution to be improved without changing the result. In the standard static analysis of the current model, about 3,000 increments are needed in a time period of one second; thus, as shown in Table 3, the viscosity parameter is set at $5{\cdot}10^{-5}$. Damage is introduced into the CDP model in compression and tension according to

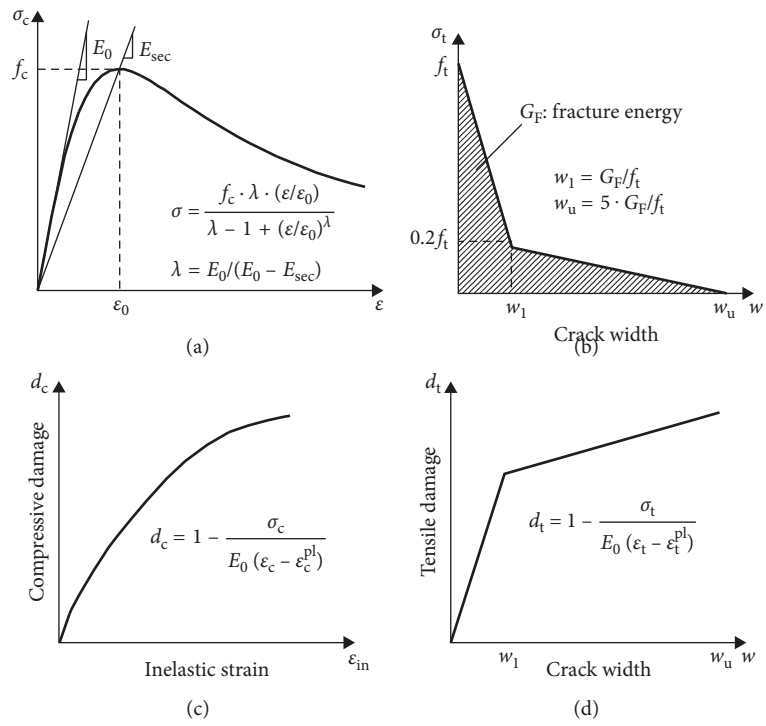

Figure 9: Constitutive laws of concrete: (a) compressive stress-strain curve, (b) tensile stress-crack width curve, (c) compressive damage-inelastic strain curve, and (d) tensile damage-crack width curve.

Table 3: Additional parameters for the CDP model.

Dilation angle	Eccentricity	f_{b0}/f_{c0}	K	Viscosity parameter
35°	0.1	1.16	0.67	$5 \cdot 10^{-5}$

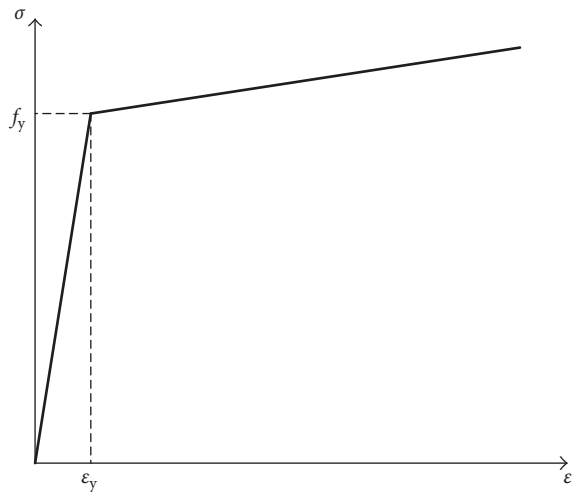

Figure 10: Stress-strain curve for the reinforcement.

Figures 9(c) and 9(d). The shape function of the unloading and reloading of compressive concrete suggested by Birtel and Mark [37] is applied to determine the evolution of the compressive damage d_c. A tensile damage-displacement curve is used to be coherent with the tension softening curve of concrete [27].

As shown in Figure 10, linear hardening is introduced to simulate the behavior of reinforcement after its yielding [26]. The material mechanical parameters used in the FE models are the same as the tested ones, which have been shown in Table 1. The elastic modules of reinforcement are set as 200 (GPa). ABAQUS/standard static analyses are applied for all the FE models.

4.2. Calibration of the FE Model. The test result of MEM-2 is used to calibrate the FE model in terms of torque-rotation curve, crack pattern, and failure mode. Referring to Figure 7, the rotation at the midspan is obtained by $\alpha = \arctan((U_{22} - U_{21})/(D_{12} + U_{11} - U_{12}))$, where the first subscript of U means the direction of displacement and the second subscript means RP1 or RP2. D_{12} is the original distance between RP1 and RP2. The applied torque is calculated by $T = F_r(D_{12+}U_{11} - U_{12})$, where F_r is the average value of the two reaction forces at RP1 and RP2. At the outset, it is essential to discuss the chosen material parameters, the mesh size, and the element type. Since it is known that a larger viscosity parameter will improve the solution but gives a stiffer response [26, 30, 34], the chosen viscosity parameter should be calibrated. As shown in Figure 11(a), the simulated torque-rotation curves with a series of viscosity parameters are compared with each other as well as with the test result. It can be seen that the viscosity parameters of $2 \cdot 10^{-5}$, $5 \cdot 10^{-5}$(used in this paper), and $10 \cdot 10^{-5}$ give almost the same results, which are accurate compared with the test results. With the increase of the viscosity parameter to

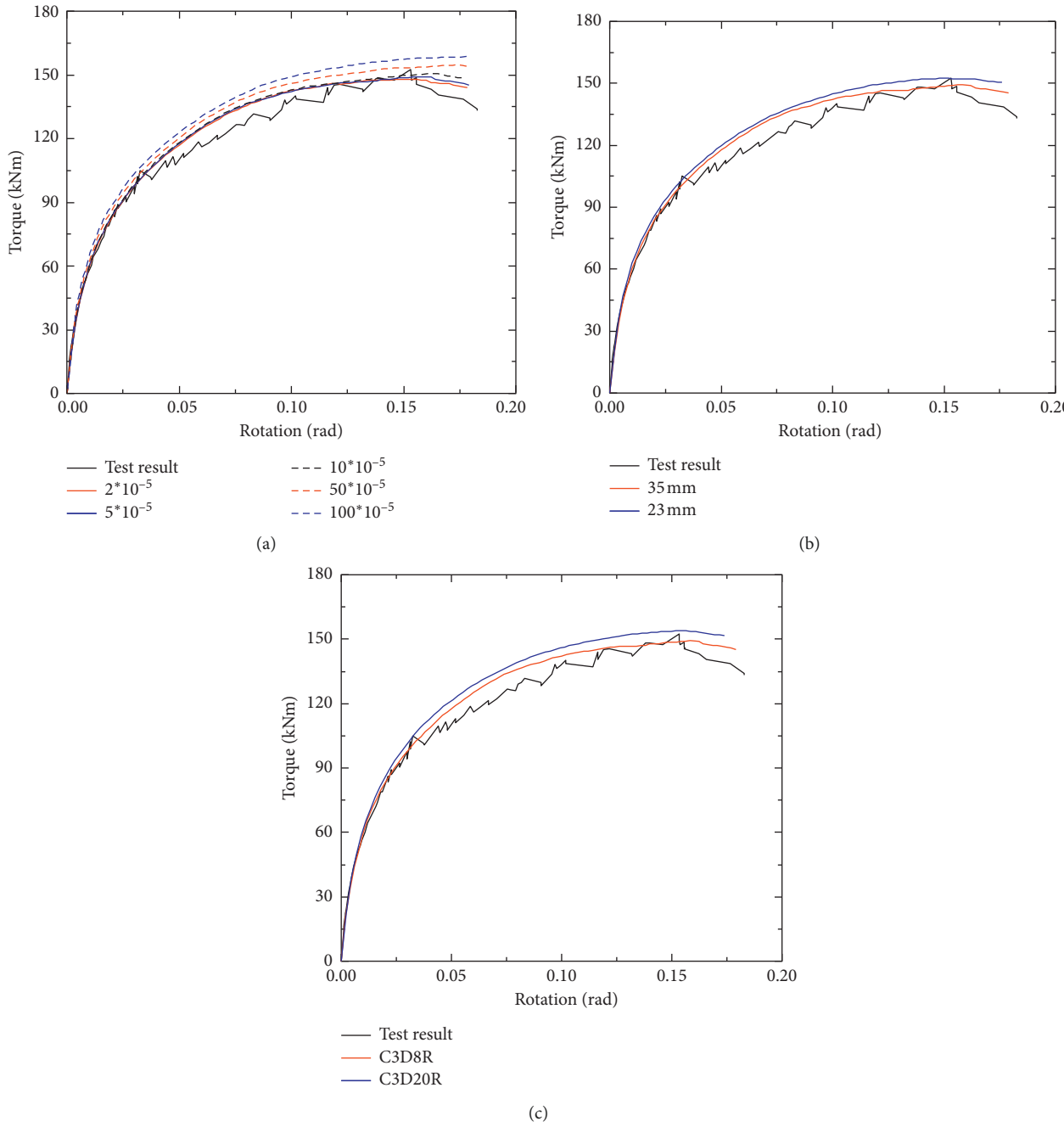

Figure 11: Torque-rotation curves with (a) different viscosity parameters, (b) different mesh sizes, and (c) different element types.

$50 \cdot 10^{-5}$ and $100 \cdot 10^{-5}$, stiffer responses are as expected. The chosen viscosity parameter of $5 \cdot 10^{-5}$ is proved to be accurate. Due to the localization of the concrete tensile cracks, the FE model is mesh size dependent as happens in most plasticity-based FE models with strain softening [26, 27, 30]. Hence, a mesh convergence study is performed. As shown in Figure 11(b), two mesh sizes of 35 mm and 23 mm were compared with each other to investigate the mesh sensitivity (35 mm mesh size giving two elements through the thickness of the thin wall while 23 mm mesh size giving three). It can be seen from Figure 11(b) that similar responses are obtained for the two mesh sizes, and they are accurate compared with the test result. Considering the computing cost, larger mesh size of 35 mm is selected. Comparison between simulated results with different element types is shown in Figure 11(c). Elements C3D20R are used to obtain the correct solution. It can be seen from Figure 11(c) that elements C3D8R and C3D20R give similar simulation results.

The simulated crack pattern and failure mode are shown in Figures 12(a) and 12(b), respectively, where the simulated crack pattern is approximately represented by the distribution of concrete tensile damage (DAMAGET) and the simulated failure mode is represented by the distribution of

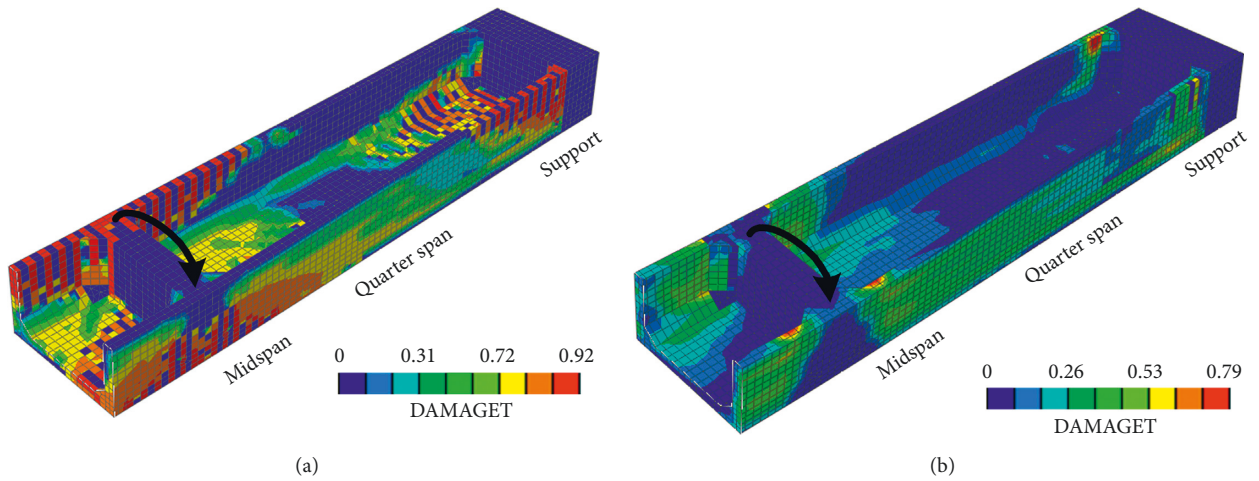

Figure 12: The simulated crack patterns and failure modes: (a) distribution of tensile damage at a load level of 80% ultimate torque and (b) distribution of compressive damage at ultimate load level. "FC" means flexural cracking, "YL" means yielding of longitudinal bars, and "YS" means yielding of stirrups.

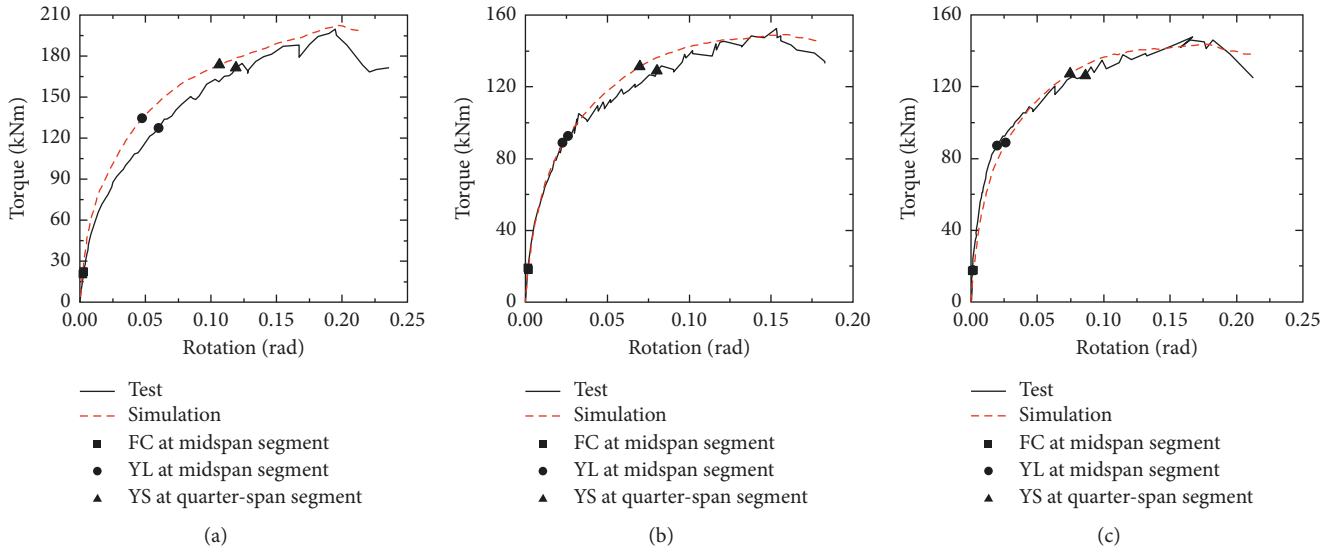

Figure 13: Simulated and tested torque-rotation curves: (a) MEM-1, (b) MEM-2, and (c) MEM-3.

concrete compressive damage (DAMAGEC). Comparing Figure 12(a) with Figure 8, it can be seen that the propagation and distribution of cracks are well simulated by the built FE model (detail features are stated in Section 3). Comparing Figure 12(b) with Figure 8, it can be observed that the distribution of DAMAGEC agrees well with the test result. The maximum DAMAGEC occurs at midspan on the top of the downward web and at the support on the top of the upward web, and those were the locations where concrete crushing occurred in the test. Flexural failure dominated by the warping moment occurred both in the simulation and in the test. From the above comparisons between the simulated results and the test results, it can be concluded that the FE model in this paper can accurately simulate the mixed torsional behavior of the tested specimen. The simulated torque-rotation curves of all the three girder specimens are shown in Figure 13.

5. Parametric Study

A parametric study considering three crucial parameters, boundary condition (fixed-fixed or simply supported), span length-characteristic length ratio, and the ratio of longitudinal bars to stirrups, is conducted. The design of the simple supporting is shown in Figure 14, where the coupling constraint with the continuum distributing and linear weighting method is used between a reference point and its slave surface. Then, the displacements in the Y direction (U_2) are restrained for the reference points on the top and at the bottom, while the displacements in the X direction (U_1) are restrained for the reference points on the two sides. In this supporting design, the displacements of the girder end in the X and Y directions (U_1 and U_2) are restrained while the displacement in the Z direction (U_3) is free; as to the rotational freedoms, the rotation of the girder end around the

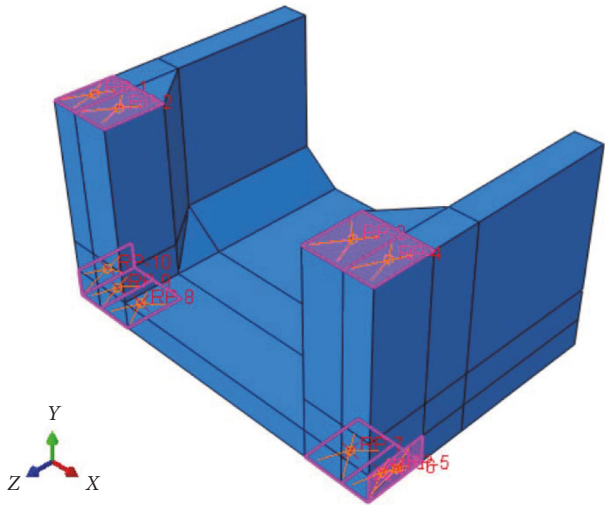

Figure 14: Design of the simple supporting.

Z direction (UR_3) is restrained while the other two rotations, UR_1 and UR_2, are free.

5.1. Effect of Span Length-Characteristic Length Ratio. As discussed in Section 2.1 with the changing of span length-characteristic length (SL-CL) ratio, different failure types may occur. The mixed torsional behaviors of these girders with varying span length-characteristic length (SL-CL) ratios are investigated here. For the fixed-fixed supported cases, the SL-CL ratio is designed to have a range of from 2.0 to 5.0 (the corresponding span length-section height ratio is from 8.2 to 20.6), and for the simply supported cases, it is from 2.0 to 4.0 (the corresponding span length-section height ratio is from 8.2 to 16.5). The above specified ranges for the SL-CL ratio should have covered all the engineering practices [2]. The numerical package of MEM-2 is applied here. The simulated torque versus midspan rotation curves for the fixed-fixed supported cases and for the simply supported cases are shown in Figures 15(a) and 15(b), respectively. The simulated results with the largest concrete compressive damage (DAMAGEC) at flexural critical segments (for fixed-fixed supported cases at midspan and support; for simply supported cases at midspan) are plotted with solid lines, while those with largest DAMAGEC at shear critical segments (for fixed-fixed supported cases at quarter segment; for simply supported cases at support) are plotted with dashed lines. Two typical simulated results with largest DAMAGEC at shear critical segments are shown in Figures 16(a) and 16(b). It can be seen from Figures 15(a) and 15(b) that, with the increase of span length, the ultimate torque drops while the ultimate rotation goes up.

Theoretically the simulated failure type can be determined by the distribution of DAMAGEC, namely, the place where the concrete is first crushed gets the maximum DAMAGEC. However, considering that the shear failure is brittle [3], in this paper, the shear failure is also determined by the yielding of stirrups and longitudinal bars at shear critical segments. Therefore, to determine which kind of failure occurs, the following criterion is applied. When the DAMAGEC at shear critical segment is larger than or as large as the DAMAGEC at bending critical segment, it is classified as a shear failure; if not, check the stress condition of reinforcement at shear critical segment: if both the stirrups and the longitudinal bars yield, it is defined as a flexural-shear failure (which means flexural failure and shear failure occur simultaneously); or if either the stirrups or the longitudinal bars at shear critical segment do not yield, it is classified as a flexural failure. According to the criterion, the simulated failure modes are summarized in Figure 15(c). The calculated results based on the calculating method developed in Section 2.2 are also shown in Figure 15(c). It can be seen from Figure 15(c) that the calculating method can give a good prediction for the failure modes as well as the ultimate torques. As shown in Figure 15(c) for the fixed-fixed supported cases, shear failure dominated by the warping torque occurs when the span length is small (SL-CL ratio 2.0). With the increase of span length to medium values (SL-CL ratios from 3.0 to 4.0), flexural failure dominated by the warping moment occurs, and when the span length further increases to 4.5 times the characteristic length, flexural-shear failures are observed. As for the simply supported cases, with the increasing of span length from 2.0 times to 4.0 times the characteristic length, the failure changes from flexural-shear type to shear type. The evolutions of failure type agree well with the expectations in Section 2.1.

It should be mentioned that ductile behaviors are observed even in flexural-shear failure cases and in shear failure cases. It can be explained by that, as shown in Figures 15(a) and 15(b), the longitudinal bars at midspan (flexure critical segment) always yield first even in flexural-shear failure cases and shear failure cases. Besides, it should be explained that the negative stiffness behaviors in the simply supported SL-CL 3.5 and SL-CL 4.0 cases (Figure 15(b)) are due to the intensive shear cracking caused by circulatory torque T_c. This negative stiffness behavior due to intensive shear cracking has been often observed in the circulatory torsional tests [10, 14, 15].

5.2. Effect of Boundary Condition. The comparison of torque-rotation curves under different boundary conditions are plotted in Figures 17(a)–17(c), respectively. It can be seen from Figures 17(a)–17(c) that when the boundary condition is changed from fixed-fixed supporting to simple supporting, the ultimate torques decreased dramatically while the ultimate rotations increased significantly. Besides, as shown in Figure 15(c), when the span length is 3.5 times the characteristic length, for the fixed-fixed supported case, flexural failure dominated by the warping moment occurs, while for the simply supported case, shear failure dominated by circulatory torque occurs. It can be concluded from both calculated results and simulated results shown in Figure 15(c) that the evolution of the failure type with the increasing of the span length is faster in the simply supported case than in the fixed-fixed supported case.

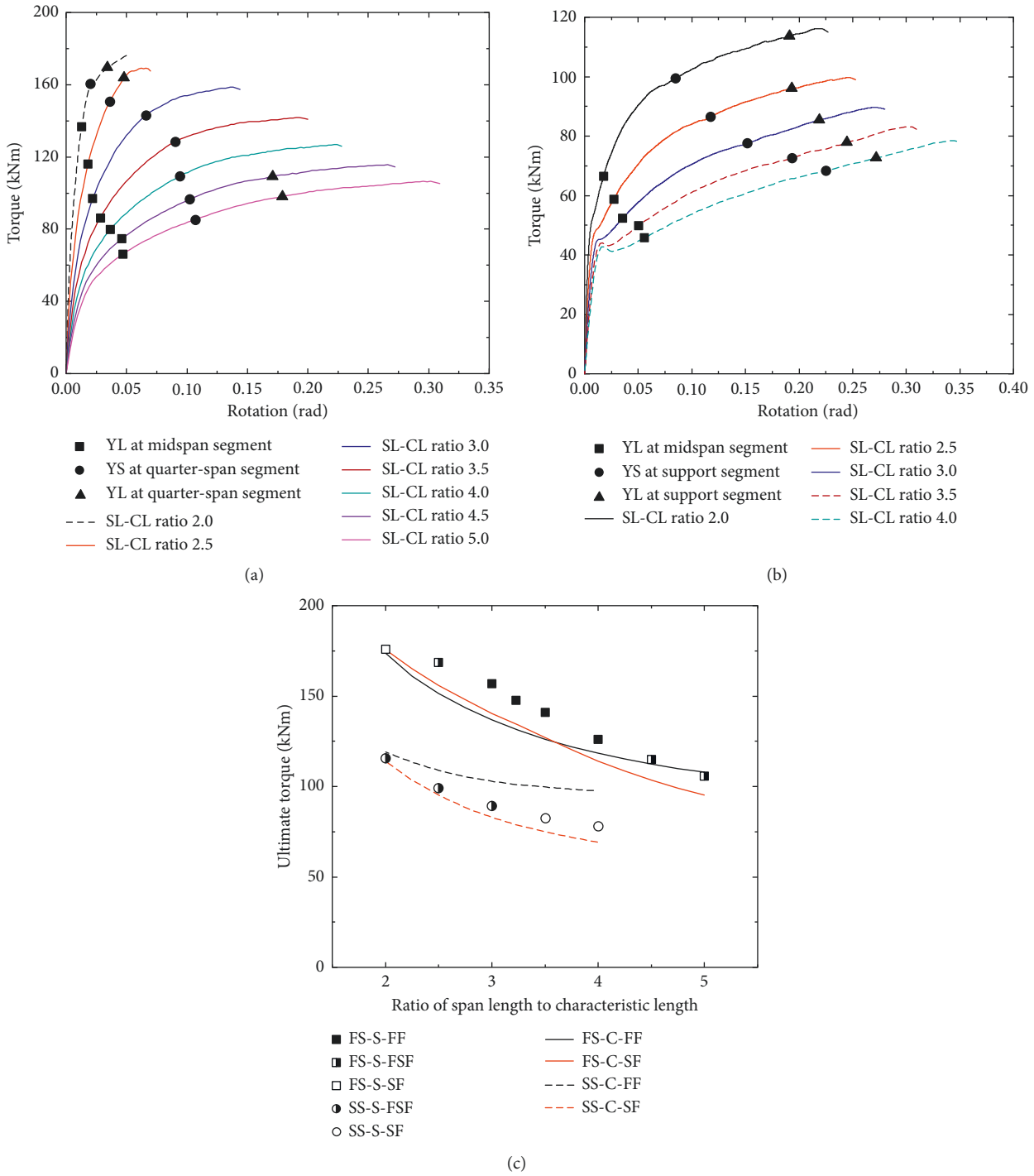

Figure 15: Simulated and calculated results of girders with various span lengths under different boundary conditions: (a) torque-rotation curves under fixed-fixed supporting, (b) torque-rotation curves under simple supporting, and (c) simulated and calculated failure modes and ultimate torques. In (a) and (b), "SL-CL ratio" means span length-characteristic length ratio; "YL" and "YS" mean yielding of longitudinal bars and yielding of stirrups, respectively. In (c), the first abbreviation "FS" and "SS" means fixed-fixed supported and simply supported, respectively; the second abbreviation "C" and "S" means calculated and simulated, respectively; and the third abbreviation "FF," "SF," and "FSF" means flexural failure, shear failure, and flexural-shear failure, respectively.

5.3. Effect of Ratio of Longitudinal Bars to Stirrups. As indicated by the calculating method in Section 2.2, the ultimate torque in a flexural failure depends mainly on the longitudinal bars while the ultimate torque in a shear failure depends on both longitudinal bars and stirrups. Thus, it can be expected that the mixed torsional behavior of the U-shaped thin-walled RC girders varies with different reinforcement ratios. The numerical package of MEM-2 is applied here to do the parametric study. For MEM-2, the original reinforcement ratio is 2.0 ($\rho_l f_{ly}/\rho_t f_{ty} = 2.0$), and flexural failure occurred. In

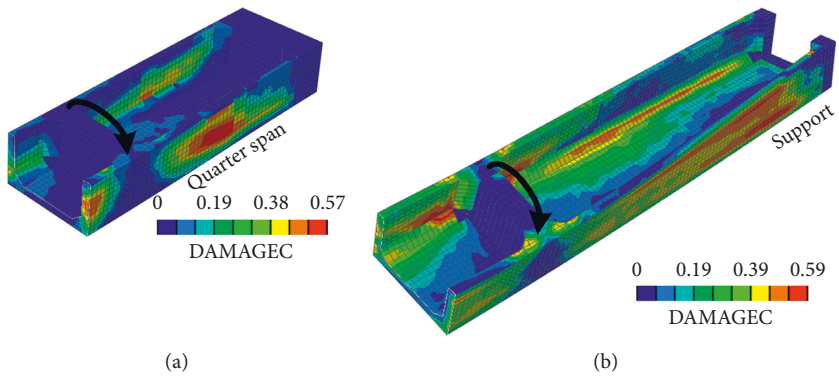

Figure 16: Two typical simulated results with the largest DAMAGEC at shear critical segment: (a) fixed-fixed supported SL-CL ratio 2.0 case and (b) simply supported SL-CL ratio 3.5 case.

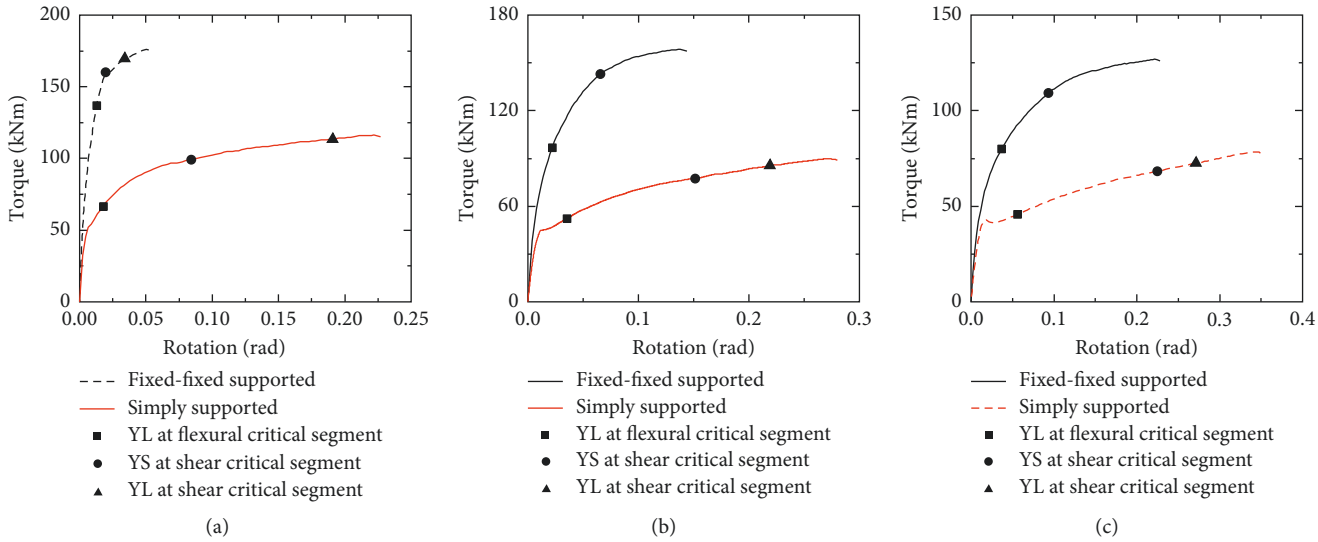

Figure 17: Simulated torque-rotation curves under different boundary conditions with (a) SL-CL ratio of 2.0, (b) SL-CL ratio of 3.0, and (c) SL-CL ratio of 4.0. "SL-CL ratio" means span length-characteristic length ratio; "YL" means yielding of longitudinal bars; "YS" means yielding of stirrups.

this parametric study, the section area of stirrups is kept constant and the section area of longitudinal bars is increased to 120%, 140%, 160%, and 180% (corresponding reinforcement ratios: 2.4, 2.8, 3.2, and 3.6) as well as decreased to 80% (the corresponding reinforcement ratio of 1.6). The corresponding simulated torque-rotation curves are shown in Figure 18(a), while the simulated failure modes and ultimate torques together with the calculation results are shown in Figure 18(b). As shown in Figure 18(b), both calculation and simulation give the same results that when the reinforcement ratio is not larger than 2.0, flexural failure occurs. With the increase of the section area of longitudinal bars, flexural-shear failure and then shear failure occur.

5.4. Comparison of the Calculated and the Simulated Torque Capacities. The calculated and simulated ultimate torques for all the above parametrically studied cases are compared in Table 4. Considering that the characteristic length (k = 2.06 m) in the above parametrically studied cases is constant, as shown in Figure 19, another two characteristic lengths of 1.8 m and 2.5 m are designed. The designed values of the characteristic length should have covered the practical engineering range [2]. Then the numerical package of MEM-2 is applied to simulate the mixed torsional behaviors of girders with various characteristic values. A fixed-fixed supported case and a simply supported case were studied for each characteristic length, with setting the span length at 3.5 times the characteristic length. The simulated results are shown in Figure 20. The simulated and calculated ultimate torques of these 4 cases are also compared in Table 4. As shown in Table 4, an average value of 1.08 for the simulation/calculation with a coefficient of variation of 5.6% proves that the calculating method can give good predictions for the torque capacities.

6. Distributions of Shear Stress Resultant

The distributions of shear stress resultant around the shear critical section at different loading levels are investigated.

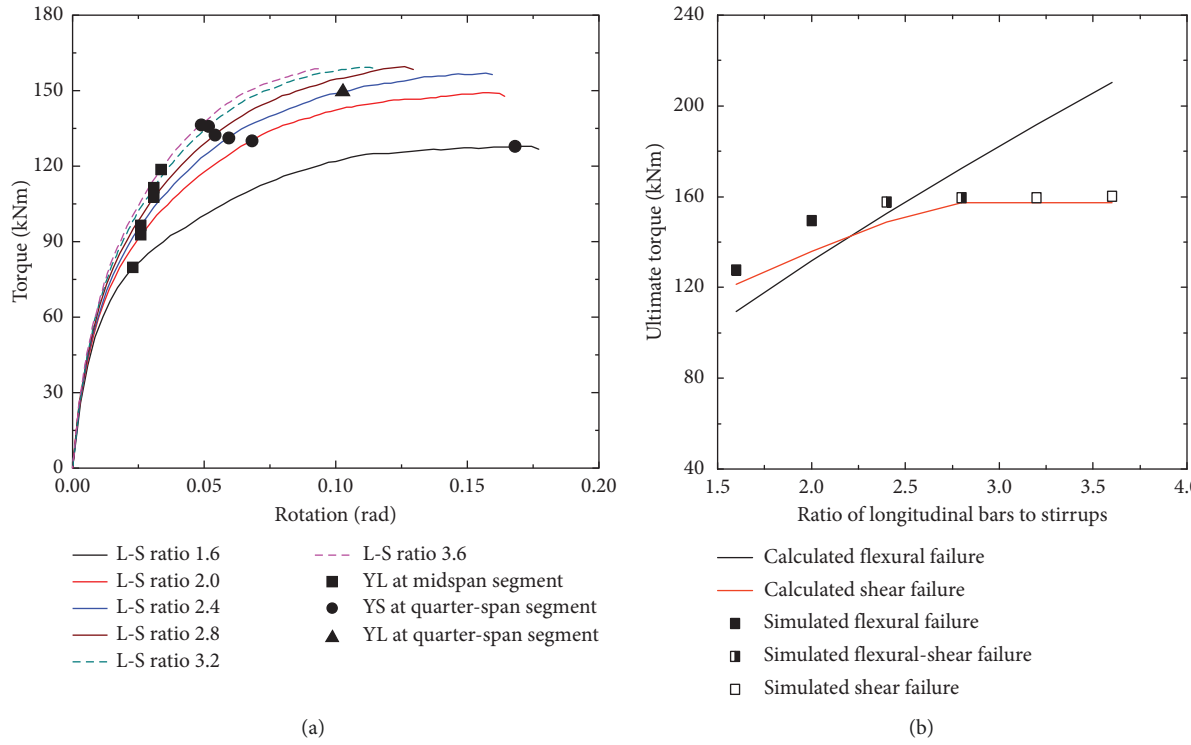

Figure 18: Simulated and calculated results considering different reinforcement ratios: (a) simulated torque-rotation curves and (b) simulated and calculated ultimate torques. "L-S ratio" means the ratio of longitudinal bars to stirrups; "YL" and "YS" mean yielding of longitudinal bars and yielding of stirrups, respectively.

Table 4: Comparison of the simulated and calculated ultimate torques.

Parametrically studied cases		Ultimate torque (kNm)		Simulation/calculation
		Simulation	Calculation	
Fixed-fixed supported cases with varying span length (Figure 15)	SL-CL ratio 2.0	176.4	174.3	1.01
	SL-CL ratio 2.5	169.2	152.2	1.11
	SL-CL ratio 3.0	157.6	137.5	1.15
	SL-CL ratio 3.5	141.7	126.8	1.12
	SL-CL ratio 4.0	126.8	114.7	1.11
	SL-CL ratio 4.5	115.6	104.2	1.11
	SL-CL ratio 5.0	106.4	95.7	1.11
Simply supported cases with varying span length (Figure 15)	SL-CL ratio 2.0	116.2	114.7	1.01
	SL-CL ratio 2.5	99.8	95.7	1.04
	SL-CL ratio 3.0	89.7	83.5	1.07
	SL-CL ratio 3.5	83.2	75.4	1.10
	SL-CL ratio 4.0	78.6	69.9	1.12
Cases with varying ratios of longitudinal bars to stirrups (Figure 18)	L-S ratio 1.6	127.8	109.5	1.17
	L-S ratio 2.0	149.5	133.1	1.12
	L-S ratio 2.4	157.7	148.8	1.06
	L-S ratio 2.8	159.5	157.5	1.01
	L-S ratio 3.2	159.7	157.5	1.01
	L-S ratio 3.6	160.2	157.5	1.02
Cases with the characteristic length of 1.8 m (Figure 20)	Fixed-fixed supported	130.3	120.2	1.08
	Simply supported	79.4	71.1	1.12
Cases with the characteristic length of 2.5 m (Figure 20)	Fixed-fixed supported	149.3	134.8	1.11
	Simply supported	98.7	90.5	1.09
Average value				1.08
Standard deviation				0.06
Coefficient of variation				5.6%

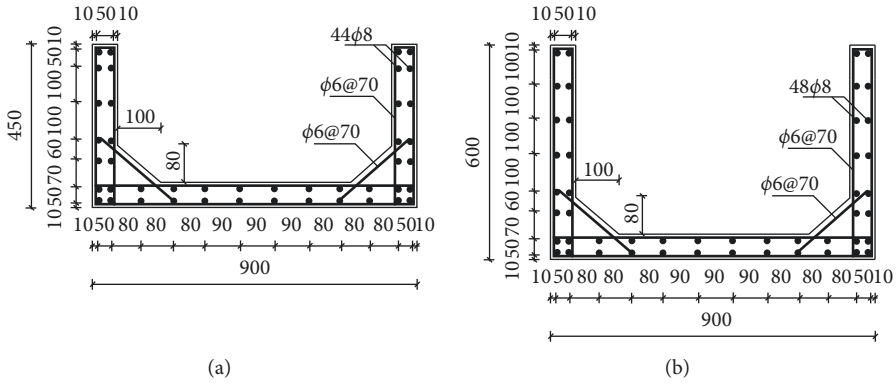

Figure 19: Girders with various characteristic lengths of (a) 1.8 m and (b) 2.5 m.

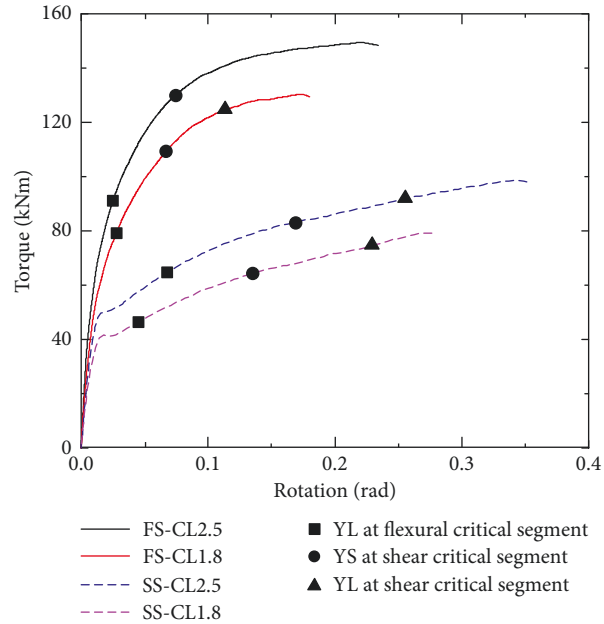

Figure 20: Simulated results of girders with various characteristic lengths. "FS" and "SS" mean "fixed-fixed supported" and "simply supported," respectively; "YL" and "YS" mean "yielding of longitudinal bars" and "yielding of stirrups," respectively.

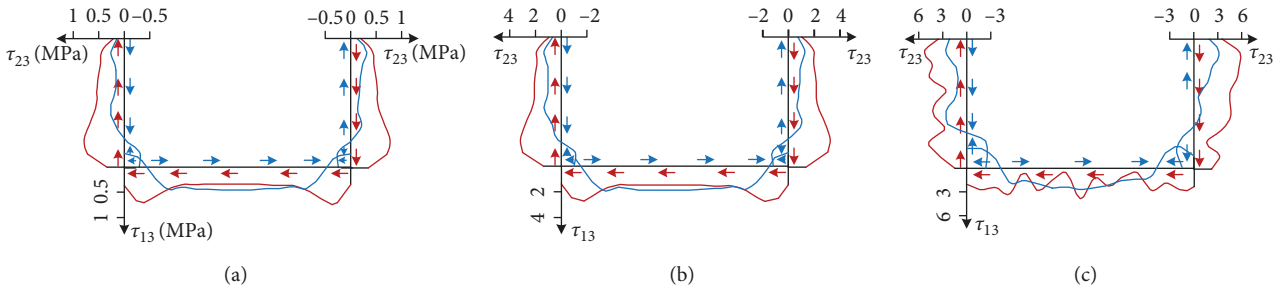

Figure 21: Shear stress distributions around quarter section at different loading levels of (a) 10% ultimate torque, (b) 30% ultimate torque, and (c) 80% ultimate torque.

The shear stress distributions of the fixed-fixed supported SL-CL ratio 3.5 case and the simply supported SL-CL ratio 3.5 case are shown in Figures 21 and 22, respectively. The direction of circulatory torsional shear stress is taken as positive. It is in the elastic range when the load level is at 10% ultimate torque. The load level of 30% ultimate torque is in the postcracking range, while the load level of 80% ultimate torque is in the postyielding range. It can be seen from Figures 21 and 22 that due to the interactions of the two kinds of shear stresses, the shear stress resultant on the

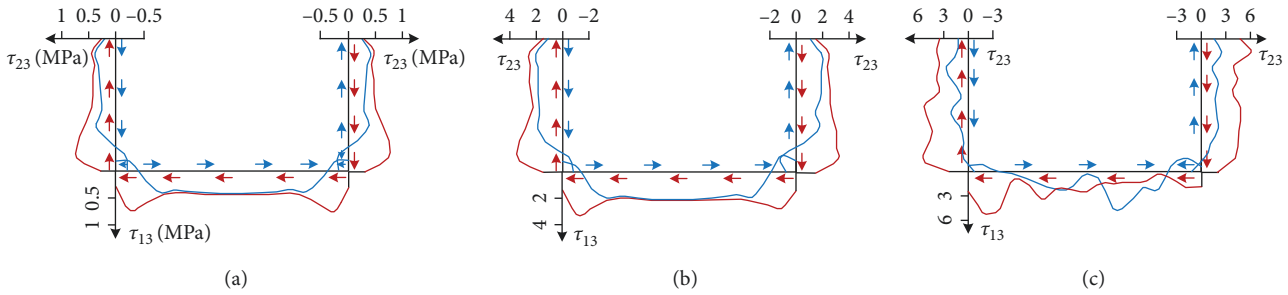

FIGURE 22: Shear stress distributions around support section at different loading levels of (a) 10% ultimate torque, (b) 30% ultimate torque, and (c) 80% ultimate torque.

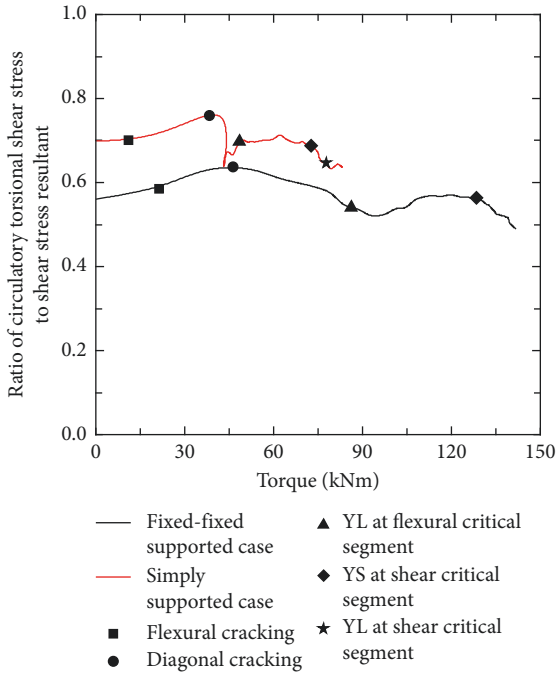

FIGURE 23: Ratio of circulatory torsional shear stress to the summation of shear stresses.

external sides of webs is larger than those on the internal sides of webs, which justifies the assumed shear stress distribution in a shear failure.

As shown in Figures 21 and 22, the shear stress resultants on the external sides of webs are the summation of the two kinds of shear stresses, while the shear stress resultants on the internal sides of webs are circulatory torsional shear stress minus warping torsional shear stress. Thus, the shear stresses caused by circulatory torque and by warping torque can be separated from each other. Then, the ratios of circulatory torsional shear stress to the summation of shear stresses can be obtained at every loading step, which is shown in Figure 23. As shown in Figure 23, this ratio fluctuated due to variation of the respective stiffness of circulatory torsion and warping torsion. For both cases in Figure 23, the ratio at the ultimate state is relatively smaller than that in the elastic range. This proves the proposed ultimate equilibrium for shear failure (the original ratio in elastic range of circulatory torque to warping torque is applied) to be conservative.

7. Conclusions

In this paper, the mixed torsional behaviors of the U-shaped thin-walled RC girders are parametrically investigated based on the theoretical analysis, the ultimate equilibrium analysis, and the nonlinear FE simulation. Three crucial parameters are considered, which are boundary condition (fixed-fixed supported or simply supported), span length-characteristic length ratio, and ratio of longitudinal bars to stirrups. This study gives a thorough understanding on the mixed torsional behavior of the U-shaped thin-walled RC girders. The conclusions are drawn in the following:

(1) The built nonlinear FE models can precisely simulate the mixed torsional behaviors of the tested U-shaped thin-walled RC girders in terms of not only the overall torque-rotation curves but also the cracking patterns and the failure modes.

(2) A method able to calculate both failure mode and ultimate torque is derived from the ultimate equilibriums at the flexural critical and shear critical segments. The calculated results are in good agreement with the test results and with the simulated results.

(3) The evolution of failure type with the increasing of span length is theoretically discovered and numerically verified: when the span length-characteristic length ratio γ is small, shear failure dominated by warping torque may occur; when γ has a medium value, flexural failure dominated by warping moment may occur; when γ has a large value, shear failure dominated by circulatory torque may occur. Besides, the evolution of failure type with the increasing of span length is faster in the simply supported case than that in the fixed-fixed supported case.

(4) The failure mode is also influenced by the reinforcement ratio between longitudinal bars and stirrups. For the specific fixed-fixed supported case with a span length of 3.23 times the characteristic length, when the reinforcement ratio is not larger than 2.0, flexural failure occurs at midspan, and as the reinforcement ratio increases, flexural-shear failure and then shear failure occur.

Notations

SL-CL Ratio (γ):	Span Length-Characteristic Length Ratio
L-S Ratio:	Ratio of Longitudinal Bars to Stirrups
I_ω:	Principal Sectorial Moment of Inertia
k:	Characteristic Length
K:	Circulatory Torsion (Saint Venant's Torsion) Constant
M_{eq}:	Equivalent Flexural Moment Acting on the Right Web of the U-Section under Warping Normal Stress
M_ω:	Warping Moment
T:	Applied Torque at the Midspan
T_c:	Circulatory Torque
T_ω:	Warping Torque
q_c:	Circulatory Torsional Shear Flow
q_ω:	Warping Torsional Shear Flow
ω:	Principal Sectorial Area.

Data Availability

The data will be shared when the paper is published. Or they are available from the corresponding author upon request.

Conflicts of Interest

The authors declare that they have no conflicts of interest.

Acknowledgments

The scholarship funded by the China Scholarship Council (CSC) with No. 201706020108 for the first author to study at the University of Houston is appreciated. This study was funded by the National Natural Science Fund (NSF) of China (Grant Nos. 51778032 and 51278020) and the Texas Department of Transportation (Project No. 0-6914).

References

[1] C.-S. Hwang and T. T. Hsu, "Mixed torsion analysis of reinforced concrete channel beams-a fourier series approach," *ACI Journal Proceedings: ACI*, vol. 80, no. 5, 1983.

[2] E. He, "Application of channel girders in project of urban rail transit," *Journal of Railway Engineering Society*, vol. 2, pp. 13–16, 2003.

[3] S. Chen, B. Diao, Q. Guo, S. Cheng, and Y. Ye, "Experiments and calculation of U-shaped thin-walled RC members under pure torsion," *Engineering Structures*, vol. 106, pp. 1–14, 2016.

[4] J. Xu, S. Chen, Q. Guo, Y. Ye, B. Diao, and Y. Mo, "Experimental and analytical studies of U-shaped thin-walled RC beams under combined actions of torsion, flexure and shear," *International Journal of Concrete Structures and Materials*, vol. 12, no. 1, p. 33, 2018.

[5] V. Z. Vlasov, *Thin-walled Elastic Beams: Office of Technical Services*, U.S. Department of Commerce, Washington, DC, USA, 1961.

[6] R. E. Erkmen and M. Mohareb, "Torsion analysis of thin-walled beams including shear deformation effects," *Thin-Walled Structures*, vol. 44, pp. 1096–1108, 2006.

[7] C. F. Kollbrunner and K. Basler, *Torsion in Structures: An Engineering Approach*, Springer Science and Business Media, Berlin, Germany, 2013.

[8] M. Aminbaghai, J. Murin, J. Hrabovsky, and H. A. Mang, "Torsional warping eigenmodes including the effect of the secondary torsion moment on the deformations," *Engineering Structures*, vol. 106, pp. 299–316, 2016.

[9] D. Mitchell and M. P. Collins, "Diagonal compression field theory-a rational model for structural concrete in pure torsion," *ACI Journal Proceedings: ACI*, vol. 71, no. 8, pp. 396–408, 1974.

[10] T. T. Hsu and Y. Mo, "Softening of concrete in torsional members-theroy and tests," *ACI Journal Proceedings: ACI*, vol. 82, no. 3, pp. 290–303, 1985.

[11] K. N. Rahal and M. P. Collins, "Analysis of sections subjected to combined shear and torsion-a theoretical model," *ACI Structural Journal*, vol. 92, 1995.

[12] K. Rahal and M. P. Collins, "Combined torsion and bending in reinforced and prestressed concrete beams," *ACI Structural Journal*, vol. 100, pp. 157–165, 2003.

[13] K. N. Rahal and M. P. Collins, "Compatibility torsion in spandrel beams using modified compression field theory," *ACI Structural Journal*, vol. 103, pp. 328–338, 2006.

[14] C.-H. Jeng and T. T. Hsu, "A softened membrane model for torsion in reinforced concrete members," *Engineering Structures*, vol. 31, no. 9, pp. 1944–1954, 2009.

[15] T. T. Hsu and Y.-L. Mo, *Unified Theory of Concrete Structures*, John Wiley & Sons, Hoboken, NJ, USA, 2010.

[16] C. H. Jeng, "Unified softened membrane model for torsion in hollow and solid reinforced concrete members: modeling precracking and postcracking behavior," *Journal of Structural Engineering*, vol. 141, no. 10, article 4014243, 2015.

[17] B. Eltaly, A. Saka, and K. Kandil, "FE simulation of transmission tower," *Advances in Civil Engineering*, vol. 2014, Article ID 258148, 13 pages, 2014.

[18] T. G. Mondal and S. S. Prakash, "Nonlinear finite-element analysis of RC bridge columns under torsion with and without axial compression," *Journal of Bridge Engineering*, vol. 21, no. 2, article 4015037, 2016.

[19] C. H. Luu, Y. L. Mo, and T. T. C. Hsu, "Development of CSMM-based shell element for reinforced concrete structures," *Engineering Structures*, vol. 132, pp. 778–790, 2017.

[20] B. Luccioni, J. Reimundin, R. Danesi, and S. Venant, "Prestressed concrete I-beams under comined mixed torsion, flexure and shear," *Proceedings of the Institution of Civil Engineers*, vol. 91, no. 3, pp. 577–592, 1991.

[21] K. Zbirohowski-Koscia, "Stress analysis of cracked reinforced and prestressed concrete thin-walled beams and shells," *Magazine of Concrete Research*, vol. 20, no. 65, pp. 213–220, 1968.

[22] P. Krpan and M. P. Collins, "Testing thin-walled open RC structure in torsion," *Journal of the Structural Division*, vol. 107, pp. 1129–1140, 1981.

[23] P. Krpan and M. P. Collins, "Predicting torsional response of thin-walled open RC members," *Journal of the Structural Division*, vol. 107, pp. 1107–1127, 1981.

[24] L. Elfgren, I. Karlsson, and A. Losberg, "Torsion-bending-shear interaction for concrete beams," *Journal of the Structural Division*, vol. 100, pp. 1657–1676, 1974.

[25] S. Chen, Y. Ye, Q. Guo, S. Cheng, and B. Diao, "Nonlinear model to predict the torsional response of U-shaped thin-walled RC members," *Structural Engineering and Mechanics*, vol. 60, no. 6, pp. 1039–1061, 2016.

[26] J. Henriques, L. S. D. Silva, and I. B. Valente, "Numerical modeling of composite beam to reinforced concrete wall joints : part I: calibration of joint components," *Engineering Structures*, vol. 52, pp. 747–761, 2013.

[27] A. S. Genikomsou and M. A. Polak, "Finite element analysis of punching shear of concrete slabs using damaged plasticity model in ABAQUS," *Engineering Structures*, vol. 98, pp. 38–48, 2015.

[28] GB50010, *Technical Specification for Concrete Structures of Tall Building*, China Construction Industry Press, China, 2010.

[29] 318 AC, *Building Code Requirements for Structural Concrete (ACI 318-14)*, American Concrete Institute, Farmington Hills, MI, USA, 2014.

[30] ABAQUS, *Abaqus Analysis User's Guide*, ABAQUS, Dallas, TX, USA, 2014.

[31] J. Dourakopoulos and E. Sapountzakis, "Nonlinear dynamic analysis of plates stiffened by parallel beams with deformable connection," *Advances in Civil Engineering*, vol. 2014, Article ID 942763, 22 pages, 2014.

[32] J. Lubliner, J. Oliver, S. Oller, and E. Oñate, "A plastic-damage model for concrete," *International Journal of Solids and Structures*, vol. 25, no. 3, pp. 299–326, 1989.

[33] J. Lee and G. L. Fenves, "Plastic-damage model for cyclic loading of concrete structures," *Journal of Engineering Mechanics*, vol. 124, no. 8, pp. 892–900, 1998.

[34] J. Lee and G. L. Fenves, "A plastic-damage concrete model for earthquake analysis of dams," *Earthquake Engineering and Structural Dynamics*, vol. 27, no. 9, pp. 937–956, 1998.

[35] J. B. Mander, M. J. Priestley, and R. Park, "Theoretical stress-strain model for confined concrete," *Journal of Structural Engineering*, vol. 114, no. 8, pp. 1804–1826, 1988.

[36] CEB-FIP, *Fib Bulletin 55: Model Code 2010, Final draft*, Vol. 1, CEB-FIP, Lausanne, Switzerland, 2012.

[37] V. Birtel and P. Mark, "Parameterised finite element modelling of RC beam shear failure," in *Proceedings of ABAQUS Users' Conference*, pp. 95–108, Boston, MA, USA, 2006.